AIP | Journal of Applied Physics

Valence fluctuation and electron–phonon coupling in La68xCexAl10Cu20Co2 (x = 0, 34, and 68) metallic glasses

M. B. Tang, J. Q. Wang, W. H. Wang, L. Xia, K. C. Chan et al.

Citation: J. Appl. Phys. **108**, 033525 (2010); doi: 10.1063/1.3467516
View online: http://dx.doi.org/10.1063/1.3467516
View Table of Contents: http://jap.aip.org/resource/1/JAPIAU/v108/i3
Published by the American Institute of Physics.

Valence fluctuation and electron–phonon coupling in $La_{68-x}Ce_xAl_{10}Cu_{20}Co_2$ (x=0, 34, and 68) metallic glasses

M. B. Tang,[1,a)] J. Q. Wang,[2] W. H. Wang,[2] L. Xia,[3] K. C. Chan,[4] and J. T. Zhao[1]
[1]*Key Laboratory of Transparent and Opto-functional Inorganic Materials, Shanghai Institute of Ceramics, Chinese Academy of Sciences, Shanghai 200050, China*
[2]*Institute of Physics, Chinese Academy of Sciences, Beijing 100190, China*
[3]*Institute of Materials, Shanghai University, Shanghai 200072, China*
[4]*Department of Industrial and Systems Engineering, Advanced Manufacturing Technology Research Center, The Hong Kong Polytechnic University, Hung Hom, Hong Kong, China*

(Received 1 April 2010; accepted 22 June 2010; published online 13 August 2010)

We study the anomalous acoustic softening behavior in $La_{68-x}Ce_xAl_{10}Cu_{20}Co_2$ (x=0, 34, and 68) metallic glasses by magnetic susceptibility, thermal expansion, and specific heat at low temperatures. The Ce-based metallic glass exhibits valence fluctuation phenomenon, anomalous thermal expansion and acoustic Grüneisen parameter at low temperatures. And we provide experimental evidence of the existence of strong electron–phonon coupling in the Ce-based metallic glasses by specific heat. The anomalous acoustic and thermal properties are attributed to the valence instability in the metallic glasses. © *2010 American Institute of Physics*. [doi:10.1063/1.3467516]

I. INTRODUCTION

The valence fluctuation phenomena in rare-earth compounds present a strong challenge to solid-state physicists.[1] In the 4*f* intermediate-valence systems, the valence instability is due to the proximity of the 4*f* level of the ion to the Fermi level, and fluctuations between two different valence states $4f^n$ and $4f^{n+1}$. Strong valence fluctuations are observed in the intermetallic compounds with Ce, Yb, Sm, etc. And the hybridization of 4*f* shell with conduction electrons is believed to give rise to anomalous properties in the compounds. By magnetic susceptibility, the intermediate-valence compounds $CeIn_{3-x}Sn_x$ exhibits a maximum at low temperature due to spin fluctuation, and a € behavior above the maximum. The effective moment of $CeIn_{3-x}Sn_x$ is close to the free-ion Ce^{3+}.[2] The specific heat of the intermediate-valence compounds also shows special behavior. For example, when the lattice contribution is subtracted out by that of LaB_6, the excess specific heat of intermediate-valence SmB_6 exhibits a large broad peak.[1]

The different valence ionic radius in the compounds is greatly different, which induces large volume difference. The valence fluctuations are accompanied by large volume fluctuations. As a result, the intermediate-valence compounds display anomalous thermal expansion. For example, the thermal expansion coefficient of $CeSn_3$ is substantially larger than that of $LaSn_3$ and shows a broad peak near 130 K.[1] The anomalous thermal expansion appears related to a softening of the lattice, which has an electronic origin and reflects the peculiar state of 4*f* electrons in cerium. Severing *et al.*[3] studied the intermediate-valence compound $CePd_3$, which shows distinct softening longitudinal acoustic modes, and accounted for by introducing an extra "breathing term" in the model calculation. The anomalous thermal expansion is observed in a number of crystalline alloys or compounds, and whether this involves a straightforward valence instability is open question.

In the intermediate-valence compounds, the $f^n \leftrightarrow f^{n+1}$ electronic transitions are expected to affect both the lattice constants as well as the electronic structure. One would expect rather strong electron–phonon coupling that would affect the phonon frequencies. Various models have been proposed to incorporate the electron–phonon coupling in the intermediate-valence compounds.[4–7] Ultrasonic and inelastic neutron scattering methods are extremely valuable in elucidating the electron–phonon coupling mechanism. Clementyev *et al.*[8] found the strong phonon anomalies in the intermediate-valence system CeNi and the isostructural reference compound LaNi. The comparison with LaNi shows that a pronounced softening occurs in several branches with acoustic character, which confirmed the effect of electron–phonon coupling. The full understanding of electron–phonon coupling in the intermediate-valence compounds remains to be solved.[6]

The study of Ce-based compounds is of particular interest as in this case the 4*f* shell contains just one electron, which may help us to explain this system with relative ease, as intra-4*f* electron interactions can be ignored. Ce-based bulk metallic glasses (BMGs) have excellent glass-forming ability, small elastic moduli, and an exceptionally low glass transition temperature.[9–11] Under high pressure, Ce-based BMG, unlike other BMGs with normal mode stiffening, exhibits an anomalous softening acoustic modes, i.e., the negative pressure derivatives of acoustic velocities or elastic constants.[12] Zhang *et al.*[12] studied the acoustic Grüneisen parameter by comparing to that of typical oxide glasses, and concluded that the anomaly in Ce-BMGs is due to the short-range covalent bonds. By the temperature-dependent acoustic properties, Ce-based BMG shows distinct softening longitudinal acoustic mode by comparing to the isostructural nonmagnetic La-based BMG.[13] In BMGs which have been

a)Electronic mail: mbtang@mail.sic.ac.cn.

found at present, the acoustic softening behavior is only observed in Ce-based amorphous alloys. The acoustic softening behavior has been studied well in crystalline alloys or compounds.[1,3,8] Whether there is same origin for the behavior in both amorphous and crystalline alloys (or compounds) is important question. In this paper, the temperature-dependent magnetization, thermal expansion, and specific heat C_p of the $La_{68-x}Ce_xAl_{10}Cu_{20}Co_2$ (x=0, 34, and 68) BMGs is studied. The results indicate that the Ce-based BMG exhibits valence fluctuation phenomenon, and anomalous thermal expansion and specific heat at low temperatures. The strong electron–phonon coupling in the BMGs is elucidated by specific heat. And the valence instability is the origin of the anomalous acoustic and thermal properties in the Ce-based BMG.

II. EXPERIMENTAL DETAILS

The $La_{68-x}Ce_xAl_{10}Cu_{20}Co_2$ (x=0, 34, and 68) BMGs were prepared and the details of the synthesis were described in Refs. 9 and 13. The glassy structure is ascertained by x-ray diffraction (XRD) and differential scanning calorimetry (DSC). The linear thermal expansion $\Delta L/L(300\ \mathrm{K})$ was measured using a foil strain gage (KYOWA; model KFL-02-120-C1). The gauge was bonded with PC-6, and measured using physical property measurement system (PPMS, Quantum Design Inc.). This method is simple but requires a material of known expansion. We used aluminum (purity: 99.99%) and the corresponding thermal expansion data of pure aluminum to calibrate the gauge.[14] Thus, although the precision of the gauges is better than 10^{-7} strain, the accuracy is only about 20%. The C_p measurements (error$<$2%) were carried out with PPMS. The dc magnetic susceptibility was measured using PPMS from 5 to 300 K.

III. RESULTS AND DISCUSSION

A. Glassy structure

Figure 1(a) shows the XRD patters of the $La_{68-x}Ce_xAl_{10}Cu_{20}Co_2$ (x=0, 34, and 68) BMGs. The samples exhibit a broad diffraction maxima characteristic of metallic glasses characterizing of amorphous structure of alloys with the limitation of the XRD. Figure 1(b) shows the glass transition, the crystallization and the melting process of the samples by DSC at heating rate of 20 K/min, which also confirms the glassy state of the $La_{68-x}Ce_xAl_{10}Cu_{20}Co_2$ (x=0, 34, and 68) BMGs.

B. Magnetic susceptibility

Figure 2 exhibits dc magnetic susceptibility M versus T for the $Ce_{68}Al_{10}Cu_{20}Co_2$ BMG along with the isostructural BMG $La_{68}Al_{10}Cu_{20}Co_2$. The reference $La_{68}Al_{10}Cu_{20}Co_2$ BMG is nonmagnetic and the $Ce_{68}Al_{10}Cu_{20}Co_2$ BMG shows paramagnetism. The inset of Fig. 2 displays the inverse dc magnetic susceptibility $1/M$ versus T for the $Ce_{68}Al_{10}Cu_{20}Co_2$ BMG. The solid lines are the fitting results by the Curie–Weiss law. In the Ce-based BMG, the Ce effective magnetic moment at high temperature is $2.89\mu_B$ by Curie–Weiss law (shown in the inset of Fig. 2), which is larger than the value $2.54\mu_B$ of the free-ion Ce^{3+}. The large Ce effective moment maybe is due to the contribution of the Co and Cu metallic elements. The inverse magnetic susceptibility $1/M$ gradually deviates Curie–Weiss law below about 80 K. The Ce effective magnetic moment below 10 K is only $1.72\mu_B$ by Curie–Weiss law (shown in the inset of Fig. 2), which is much smaller than that of the free-ion Ce^{3+}. The free-ion Ce^{4+} is nonmagnetic. The effective magnetic moment in the BMG interpolates between those of the free-ion Ce^{3+} and Ce^{4+} at low temperature, which shows that the Ce-based BMG exhibits valence fluctuation phenomena.

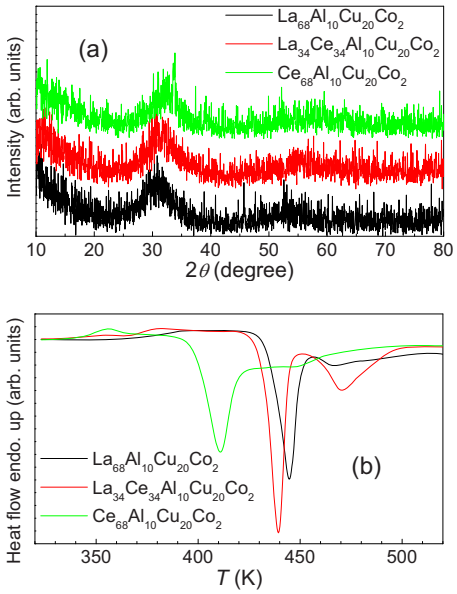

FIG. 1. (Color online) (a) XRD patterns for the $La_{68-x}Ce_xAl_{10}Cu_{20}Co_2$ (x=0, 34, and 68) BMGs; (b) DSC traces of the alloys showing the glass transition, crystallization, and the melting process. The scanning rate is 20 K/min.

C. Thermal expansion

Figure 3(a) displays the thermal expansion $\Delta L/L(300\ \mathrm{K})$ as a function temperature from 5 to 300 K for both BMGs. The $\Delta L/L(300\ \mathrm{K})$ of both BMGs exhibits a

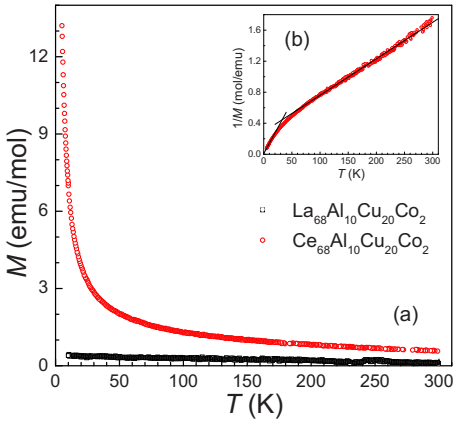

FIG. 2. (Color online) dc magnetic susceptibility M vs T for the $La_{68}Al_{10}Cu_{20}Co_2$ and $Ce_{68}Al_{10}Cu_{20}Co_2$ BMGs. Inset: inverse dc magnetic susceptibility $1/M$ vs T for the $Ce_{68}Al_{10}Cu_{20}Co_2$ BMG. The solid lines are the fitting results by the Curie–Weiss law.

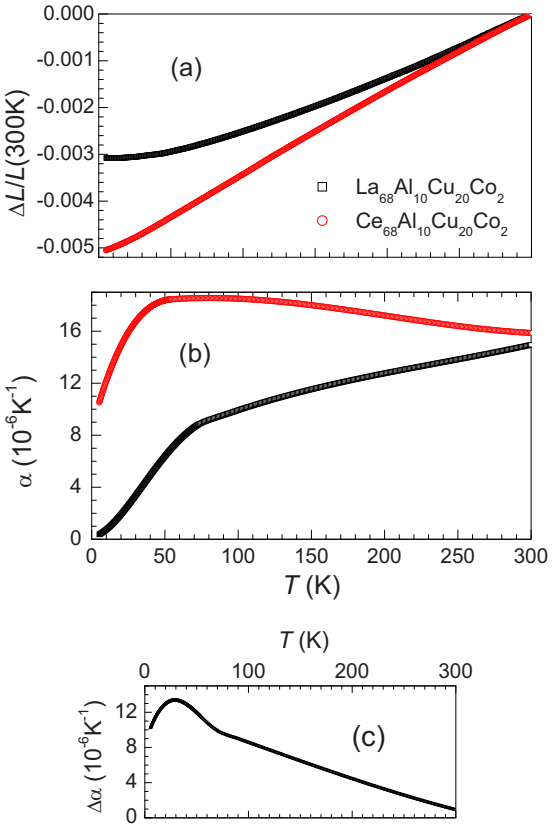

FIG. 3. (Color online) (a) Thermal expansion of the $Ce_{68}Al_{10}Cu_{20}Co_2$ BMG along with the isostructural nonmagnetic reference BMG $La_{68}Al_{10}Cu_{20}Co_2$. (b) Thermal expansion coefficient α of the $Ce_{68}Al_{10}Cu_{20}Co_2$ and $La_{68}Al_{10}Cu_{20}Co_2$ BMGs. (c) $\Delta\alpha$ vs T.

positive T-coefficient from 5 to 300 K and the effect of the thermal expansion in the $Ce_{68}Al_{10}Cu_{20}Co_2$ BMG is obvious comparing to that of the La-based BMG. Figure 3(b) shows the linear thermal expansion coefficient $\alpha = d[\Delta L/L(300\ \mathrm{K})]/dT$ of the $Ce_{68}Al_{10}Cu_{20}Co_2$ and $La_{68}Al_{10}Cu_{20}Co_2$ BMGs. We determined the α by fitting the data in Fig. 3(a) using polynomials and differentiating, as reported previously.[15] The thermal expansion coefficient α of the La-based BMG increases quickly with increasing temperature at low temperature, and is up to a constant, which is almost usual in metallic systems. The coefficient α of the Ce-based BMG is larger than that of the reference La-based BMG, and changes from 10.52×10^{-6} K^{-1} at 5.26 K to 15.87×10^{-6} K^{-1} at 300 K with an obvious hump near 50 K, which is like that of the intermediate-valence compound $CeSn_3$.[1] At 300 K, the coefficient α of the La-based BMG is 14.95×10^{-6} K^{-1}, which is close to that of the pure La (12.1×10^{-6} K^{-1}). The coefficient α of the Ce-based BMG at 300 K is 15.87×10^{-6} K^{-1}, and is larger than that of the pure Ce (6.3×10^{-6} K^{-1}). Figure 3(c) exhibits $\Delta\alpha = \alpha(\text{Ce-based BMG}) - \alpha(\text{La-based BMG})$ versus T, which increases rapidly decreasing temperature, and exhibits a peak down to 29 K.

D. Heat capacity

The measured specific heat C_p of the $La_{68-x}Ce_xAl_{10}Cu_{20}Co_2$ (x=0, 34, and 68) BMGs from 2 to 300 K is shown in Fig. 4. The specific heat of the alloys x=34 and 68 is larger than that of the alloy x=0 in the temperature range from 2 to 300 K. With the temperature increase, the specific heat C_p (molar-atom) gradually reaches a constant value [27.3 J mol^{-1} K^{-1}, 28.3 J mol^{-1} K^{-1}, and 28.4 J mol^{-1} K^{-1} at 303 K for $La_{68-x}Ce_xAl_{10}Cu_{20}Co_2$ (x=0, 34, and 68), respectively], which is larger than the classical Dulong–Petit value 24.94 J mol^{-1} K^{-1}. The C_p/T versus T^2 is plotted in the temperature range of 2 and 7.5 K (shown in the inset in Fig. 4). In the temperature range $12<T^2<56$ K^2, the data of La-based BMG is well fitted in a polynomial form $C_p/T=\gamma+\beta T^2$ with $\gamma=3.24$ mJ mol^{-1} K^{-2} and $\beta=993.6$ μJ mol^{-1} K^{-4}. The θ_D is derived to be 125 K by $\beta=(12\pi^4R/5)(1/\theta_D^3)$ (where R is the gas constant), which is close to that of the $La_{60}Cu_{20}Ni_{10}Al_{10}$ BMG.[16] And just like other BMGs,[17] in the lower temperature range $4<T^2<12$ K^2, the data is deviated from the linear behavior. The deviation in the BMG could be ascribed to the glassy state effect or tunneling state effect.[17] Due to the $4f$ electron effect, the C_p/T versus T^2 plot at low temperature for the $La_{68-x}Ce_xAl_{10}Cu_{20}Co_2$ (x=34 and 68) BMGs is obviously deviated from the linear behavior, which is close to that of the heavy fermion $Ce_xLa_{65-x}Al_{10}Cu_{20}Co_5$ (x=0, 10, 20, and 65) BMGs.[18]

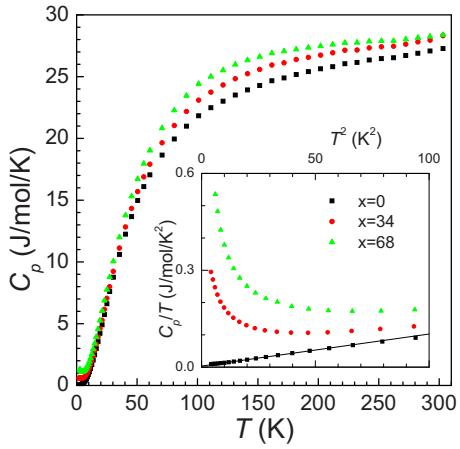

FIG. 4. (Color online) Specific heat C_p of the $La_{68-x}Ce_xAl_{10}Cu_{20}Co_2$ (x=0, 34, and 68) BMGs in the temperature range from 2 to 300 K. Inset: specific heat, shown as C_p/T vs T^2 at low temperature, the solid line is the fitting result of the specific heat between 2 and 7.5 K using the expression $C_p/T=\gamma+\beta T^2$ for $La_{68}Al_{10}Cu_{20}Co_2$ BMG.

E. Electron–phonon coupling

The excess specific heat ΔC_p of the alloys x=34 and 68 is obtained by subtracting the C_p of the $La_{68}Al_{10}Cu_{20}Co_2$ glass [Fig. 5(a)]. The excess specific heat ΔC_p of both alloys x=34 and 68 shows a peak near 100 K, and increases rapidly decreasing temperature at low temperature. The simple extrapolation in the glasses is made by drawing straight lines from the lowest temperature data point to $T=0$, $\Delta C_p=0$. The entropy of the excess specific heat for both alloys x=34 and 68 can be got by $\Delta S=\int_{T_{\min}}^{T_{\max}}(\Delta C_p/T)dT$, and is exhibited in Fig. 5(b). In the measured temperature range, ΔS is about 10.1 J/mol Ce/K and 10.3 J/mol Ce/K for both alloys x=34 and 68, respectively. The total magnetic entropy of Ce^{3+}

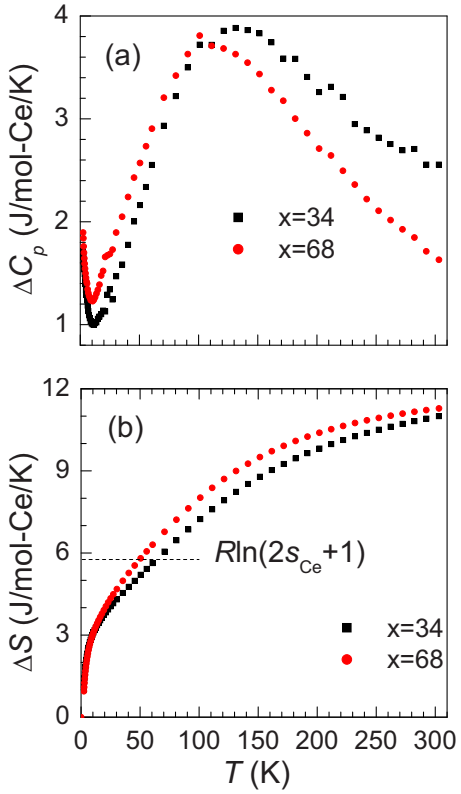

FIG. 5. (Color online) Excess specific heat ΔC_p (a) and entropy ΔS (b) of the $La_{68-x}Ce_xAl_{10}Cu_{20}Co_2$ (x=34 and 68) BMGs.

ion ($s_{Ce}=1/2$) is $\Delta S=R\ln(2s_{Ce}+1)=5.76$ J/mol Ce/K, here R is the gas constant. ΔS for both samples is thus comparable to or exceeds the total available from cerium moments and is only a lower limit. Data below the lowest temperature data point would clearly contribute to significantly more entropy. The fact that the lower limit set on the total ΔS is greater than $R\ln(2s_{Ce}+1)$ suggests that there is the contribution of strong electron–phonon coupling.

Figure 6(a) shows $\Delta C_p/T$ versus T for the $Ce_{68}Al_{10}Cu_{20}Co_2$ BMG at low temperature. In the temperature range from 2.5 to 8 K, $\ln(\Delta C_p/T)$ is linear with $\ln(T)$, which is shown by solid line in Fig. 6(a). Below 10 K, the $4f$ magnetic electron contributes mainly to specific heat due to the heavy fermion effect, and the electron–phonon coupling contributes weakly to specific heat. So the linear behavior in $\ln(\Delta C_p/T)$ versus $\ln(T)$ at low temperature is mainly due to the $4f$ electron contribution. The f electron's specific heat in the measured temperature range is got by simple extrapolation of the linear behavior, which is exhibited in Fig. 6(b). After subtracting the $4f$ electron's contribution from the total excess specific heat ΔC_p, the residual specific heat of the alloy should be the contribution of the electron–phonon coupling, which is also shown in Fig. 6(b). By the calculating results, the effect of the electron–phonon coupling is strong near 100 K.

The entropy of f electron and electron–phonon coupling for the $Ce_{68}Al_{10}Cu_{20}Co_2$ BMG is got by the specific heat of f electron and electron–phonon coupling, respectively, and is exhibited in Fig. 7. With the temperature increase, the entropy of f electron increases rapidly below about 15 K, and

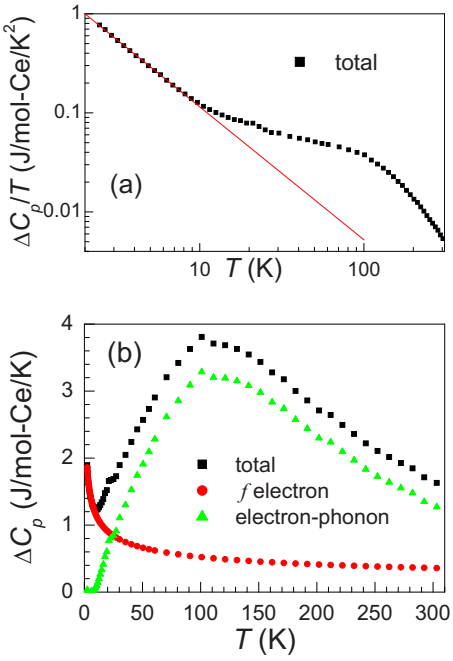

FIG. 6. (Color online) (a) $\Delta C_p/T$ vs T for the $Ce_{68}Al_{10}Cu_{20}Co_2$ BMG at low temperature; the solid line is the fitting result. (b) Specific heat of f electron and electron–phonon coupling for the $Ce_{68}Al_{10}Cu_{20}Co_2$ BMG.

gradually reaches a constant value of 5.33 J/mol Ce/K at 303 K, which is close to the total magnetic entropy of Ce^{3+} ion 5.76 J/mol Ce/K in Fig. 7. The entropy of electron–phonon coupling is weak at low temperature, and increases gradually above about 10 K.

The Ce-based amorphous alloy shows the valence instability by the low temperature physical properties, which was expected to result in a wealth of phonon anomalies because of the large volume difference between two different valence states.[1] If the volume fluctuation of the rare-earth atoms occurs on a time scale comparable with typical lattice response times, an influence on the phonon system like the damping of certain phonon modes may be expected.[3,8] As a result, one would expect rather strong electron–phonon coupling that affect the phonon frequencies in the intermediate-valence

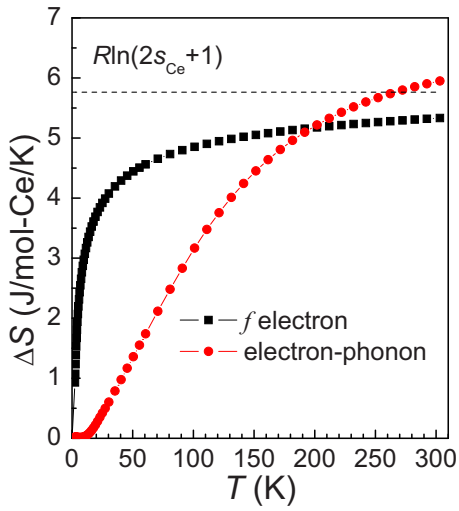

FIG. 7. (Color online) Entropy of f electron and electron–phonon coupling for the $Ce_{68}Al_{10}Cu_{20}Co_2$ BMG.

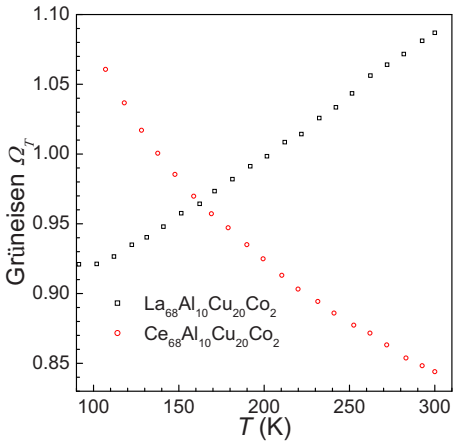

FIG. 8. (Color online) Grüneisen parameters Ω_T for the $Ce_{68}Al_{10}Cu_{20}Co_2$ and $La_{68}Al_{10}Cu_{20}Co_2$ BMGs.

compounds. The frequency distribution or the density of phonon modes determines the specific heat. In the Ce-based alloys, the electron–phonon coupling is enough strong to affect the behavior of the specific heat obviously. So specific heat is another method to elucidate the strong electron–phonon coupling mechanism.

F. Grüneisen parameter

Grüneisen parameter is an important parameter for describing anharmonic properties of solids. The thermal Grüneisen parameter can be obtained directly from the thermal expansivity α, the bulk modulus B, the unit-cell volume V_a, and the heat capacity C_p as follows: $\Omega_T=3\alpha BV_a/C_p$. The temperature-dependent bulk modulus B and the unit-cell volume V_a at room temperature of the La-based and Ce-based BMG has been measured.[13] The thermal Grüneisen parameter Ω_T of both BMGs from 90 to 300 K is shown in Fig. 8. The values of Ω_T for both BMGs are positive. At 300 K, the value of Ω_T is 1.087 and 0.844 for the La-based and Ce-based BMG, respectively. The thermal Grüneisen parameter of both BMGs shows different temperature-dependent behavior, negative for the Ce-based BMG and positive for La-based BMG, respectively. By the temperature-dependent acoustic velocity in both BMGs,[13] the longitudinal acoustic velocity shows greatly different behavior. The softening longitudinal acoustic mode maybe induces the difference of the thermal Grüneisen parameter in the La-based and Ce-based BMGs.

The Grüneisen parameter can be approximately determined by elastic data,[19] which is acoustic Grüneisen parameter. The acoustic Grüneisen parameter is not available for our specimens. The acoustic Grüneisen parameter has been measured for a material of composition ($Ce_{70}Al_{10}Ni_{10}Cu_{10}$ BMG) close to that of the present work. Like oxide glasses, the value of the acoustic Grüneisen parameter is negative (-0.23) at room temperature, which is greatly different from that of other BMGs.[12] Due to the transverse acoustic mode softening under pressure in the oxide glasses, the transverse vibration is the source of the anomalous elastic properties.[20] But in $Ce_{70}Al_{10}Ni_{10}Cu_{10}$ BMG, both of the transverse and longitudinal acoustic modes soften under pressure,[12] which induces the negative acoustic Grüneisen parameter. The acoustic softening behavior maybe plays an important role in the difference between the thermal (0.844) and acoustic (-0.23) Grüneisen parameters in Ce-based BMGs at room temperature.

IV. CONCLUSIONS

We find that the $La_{68-x}Ce_xAl_{10}Cu_{20}Co_2$ (x=34 and 68) BMGs exhibit valence fluctuation phenomenon and strong electron–phonon coupling at low temperatures. The thermal expansion coefficient α of the $Ce_{68}Al_{10}Cu_{20}Co_2$ BMG is larger than that of the $La_{68}Al_{10}Cu_{20}Co_2$ metallic glass. The Ce-based BMG exhibits anomalous specific heat behavior, which suggests the existence of the strong electron–phonon coupling in the BMGs. Comparing to the thermal Grüneisen parameter, the anomalous acoustic Grüneisen parameter is due to the acoustic modes softening. The anomalous acoustic and thermal properties may be attributed to the valence instability in the Ce-based BMG, which is important to understand the origin of the acoustic softening behavior in amorphous and crystalline alloys or compounds.

ACKNOWLEDGMENTS

The financial support of the National Science Foundation of China (Grant No. 50821004), the National Basic Research Program of China (MOST, Grant Nos. 2007CB607503 and 2007CB613904), and the MPG-CAS Partner Group Program is appreciated.

[1] J. M. Lawrence, P. S. Riseborough, and R. D. Parks, Rep. Prog. Phys. **44**, 1 (1981).
[2] J. Lawrence, Phys. Rev. B **20**, 3770 (1979).
[3] A. Severing, W. Reichardt, E. Holland-Moritz, D. Wohlleben, and W. Assmus, Phys. Rev. B **38**, 1773 (1988).
[4] O. L. T. de Menezes and A. Troper, Phys. Rev. B **22**, 2127 (1980).
[5] J. Keller, R. Bulla, Th. Höhn, and K. W. Becker, Phys. Rev. B **41**, 1878 (1990).
[6] M. Rivas, J. Rössler, and M. Kiwi, Phys. Rev. B **43**, 3593 (1991).
[7] G. C. Rout, M. S. Ojha, and S. N. Behera, Physica B **367**, 101 (2005).
[8] E. S. Clementyev, P. A. Alekseev, M. Braden, J.-M. Mignot, G. Lapertot, V. N. Lazukov, and I. P. Sadikov, Phys. Rev. B **57**, R8099 (1998).
[9] B. Zhang, M. X. Pan, D. Q. Zhao, and W. H. Wang, Appl. Phys. Lett. **85**, 61 (2004).
[10] B. Zhang, D. Q. Zhao, M. X. Pan, R. J. Wang, and W. H. Wang, Acta Mater. **54**, 3025 (2006).
[11] B. Zhang, D. Q. Zhao, M. X. Pan, W. H. Wang, and A. L. Greer, Phys. Rev. Lett. **94**, 205502 (2005).
[12] B. Zhang, R. J. Wang, and W. H. Wang, Phys. Rev. B **72**, 104205 (2005).
[13] P. Yu, R. J. Wang, D. Q. Zhao, and H. Y. Bai, Appl. Phys. Lett. **91**, 201911 (2007).
[14] F. R. Kroeger and C. A. Swenson, J. Appl. Phys. **48**, 853 (1977).
[15] J. J. Neumeier, R. K. Bollinger, G. E. Timmins, C. R. Lane, R. D. Krogstad, and J. Macaluso, Rev. Sci. Instrum. **79**, 033903 (2008).
[16] M. B. Tang, M. X. Pan, D. Q. Zhao, and W. H. Wang, J. Non-Cryst. Solids **351**, 2572 (2005).
[17] M. B. Tang, H. Y. Bai, and W. H. Wang, Phys. Rev. B **72**, 012202 (2005).
[18] M. B. Tang, H. Y. Bai, W. H. Wang, D. Bogdanov, K. Winzer, K. Samwer, and T. Egami, Phys. Rev. B **75**, 172201 (2007).
[19] O. L. Anderson, Geophys. J. Int. **143**, 279 (2000).
[20] E. F. Lambson, W. A. Lambson, J. E. Macdonald, M. R. J. Gibbs, G. A. Saunders, and D. Turnbull, Phys. Rev. B **33**, 2380 (1986).